Article

Design, Manufacturing and Test of a High Lift Secondary Flight Control Surface with Shape Memory Alloy Post-Buckled Precompressed Actuators [†]

Thomas Sinn [1] and Ron Barrett [2],*

[1] Mechanical & Aerospace Engineering Department, University of Strathclyde, Glasgow G1 1XJ, UK; E-Mail: thomas.sinn@strath.ac.uk

[2] Aerospace Engineering Department, the University of Kansas, Lawrence, KS 66045, USA

[†] This is an expanded version of conference paper: Sinn, T.; Barrett, R. Design, Manufacturing and Test of a High Lift Secondary Flight Control Surface with SMAPBP (Shape Memory Alloy Post-Buckled Precompressed) Actuators. In Proceedings of the ASME 2010 Conference on Smart Materials, Adaptive Structures and Intelligent Systems, Philadelphia, PA, USA, 28 September–1 October 2010.

* Author to whom correspondence should be addressed; E-Mail: adaptivebarrett@gmail.com; Tel.: +1-785-760-4614; Fax: +1-785-864-3597.

Abstract: The use of morphing components on aerospace structures can greatly increase the versatility of an aircraft. This paper presents the design, manufacturing and testing of a new kind of adaptive airfoil with actuation through Shape Memory Alloys (SMA). The developed adaptive flap system makes use of a novel actuator that employs SMA wires in an antagonistic arrangement with a Post-Buckled Precompressed (PBP) mechanism. SMA actuators are usually used in an antagonistic arrangement or are arranged to move structural components with linearly varying resistance levels similar to springs. Unfortunately, most of this strain energy is spent doing work on the passive structure rather than performing the task at hand, like moving a flight control surface or resisting air loads. A solution is the use of Post-Buckled Precompressed (PBP) actuators that are arranged so that the active elements do not waste energy fighting passive structural stiffnesses. One major problem with PBP actuators is that the low tensile strength of the piezoelectric elements can often result in tensile failure of the actuator on the convex face. A solution to this problem is the use of

SMA as actuator material due to their tolerance of tensile stresses. The power consumption to hold deflections is reduced by approximately 20% with the Post-Buckled Precompressed mechanism. Conventional SMAs are essentially non-starters for many classes of aircraft due to the requirement of holding the flight control surfaces in a given position for extremely long times to trim the vehicle. For the reason that PBP actuators balance out air and structural loads, the steady-state load on the SMAs is essentially negligible, when properly designed. Simulations and experiments showed that the SMAPBP actuator shows tip rotations on the order of 45 °, which is nearly triple the levels achieved by piezoelectric PBP actuators. The developed SMAPBP actuator was integrated in a NACA0012 airfoil with a flexible skin to carry out wind tunnel tests.

Keywords: smart airfoil; shape memory alloy; post-buckled precompressed

1. Introduction

For more than 20 years, adaptive materials have been regularly integrated into aerospace vehicles, structures and surfaces of many sizes. From F-14s to Boeing 787s their ability to change physical properties or state on demand has made them desirable for many different devices. Starting with simple bending- and twist-active plates in the late 1980s, some of the first rudimentary flap-type devices were seen as early as 1990 [1–4]. The first attempts at making adaptive rotors, missile fins, wings and stabilizers were also publicly exhibited in 1990 with the first patent on such devices issuing in 1995 [5–8]. These devices showed great promise and lead to numerous aeroelastic studies and development of missile fins which were capable of nontrivial deflection levels, high rates and very compact form factors [9–18]. Several early studies explored the potential for using adaptive materials on hard-launched munitions and air to ground weapon systems [19–29]. A number of helicopter rotor studies drawing their lineage back to the late 1980s and continuing through the 1990s showed fundamental utility of the piezoelectric materials as rotor blade actuators [6,7,30–32]. These many advances were shown to be "enabling" for some of the smallest aircraft commissioned by the Department of Defense (DoD). As part of the DoD CounterDrug Technology Office's remote sensing program, the DoD's first Micro Aerial Vehicle (MAV) program kicked off in 1994 and concluded with hundreds of successful flights by 1997. High bandwidths (>40 Hz), large deflections (>±10 °) and extremely low mass (<400 mg) requirements made for a challenging program [33,34]. This lead to DARPA's first MAV program which pioneered in developing both fixed and rotary-wing subscale aircraft.

Private funding continued the lineage of adaptive aircraft and resulted in the first ultra-high performance, convertible UAVs. Capable of hovering in more places than a helicopter, then dashing out at missile speeds, through 350 kts in a standard atmosphere with more than an hour of dash capability, the XQ-138 possessed performance over a decade ago that was not matched by any aircraft of its class that was sponsored by the US Federal government. As part of this study, several high performance kits were developed. In an effort to drive component weights lower with higher performance, new techniques were sought to boost piezoelectric actuator mechanical energy and power densities. One paradigm-shifting advance in this area was made in 1997 when it was discovered that with proper design,

piezoelectric elements could possess effective coupling coefficients (and therefore electrical-to-mechanical conversion efficiencies) greater than that of the basic material [35,36]. Although these basic advances were applied only to electrical transformers, their implications for flight control actuation was clear, and resulted in a number of high performance actuators. These Post-Buckled Precompressed (PBP) actuators possessed nearly four times greater deflection levels than their linear counterparts while maintaining all of the force and moment generation capability [37–41]. These actuators were integrated into speed kits for the XQ-138 aircraft which boosted flight speeds by nearly 30% while reducing flight control weight fractions by a factor of 4.8 with respect to conventional electromagnetic flight control actuators.

Although highly successful, piezoelectrically energized PBP actuators possess some profound limitations. The techniques pioneered in References [37,42] showed that through dynamic elastic axis shifting and proper control, extremely high speeds and robust performance can be achieved; however, the elements are still limited.

Following the commercial serial production of XQ-138 PBP actuators, a host of other efforts proliferated. Many of these efforts, like the concept of post-buckled precompressed actuators themselves drew their roots back to the original work of Lesieutre in the late 1990s [35,36]. This, of course, is critical to note, as it was discovered back then that the amount of mechanical strain energy and power consumed could be almost completely nulled by the application of suitable axial force levels. While the team spearheading the XQ-138 program chose to operate just below buckling levels, other groups operated just above them, leading to a host of bi-stable devices. Arrieta, Bilgen, Friswell and Hagedorn employed bi-stable morphing concepts for passive load alleviation [43]. The Friswell team continued to explore many different arrangements of flight control mechanisms including inextensible airfoils [44]. Energy harvesting was enabled by using near-buckling and bi-stable structures fitted with piezoelectric elements [45–51]. One general property that was observed in many of these studies was that with greater levels of near-buckling deflection amplification levels, hysteresis levels were increased dramatically. While the XQ-138 team simply sensed position and closed a loop to solve the problem, high end structural-mechanics models were developed to attack the open-loop variant of the problem. These general concepts were also extended to including hysteresis models and into devices using single crystal piezoelectric transducers [52–54]. Because piezoelectric macro-fiber composites could endure relatively high strain levels, they were employed in a number of flight control surfaces, some of which made it into flight quite successfully [55–59]. To enable these devices a nontrivial amount of work was done on the driving electronics (especially reducing them to flightweight levels) [60].

With limited tensile stress levels to fracture, piezoelectrically driven PBP actuators rapidly can generate so much deflection that they literally tear themselves apart. Accordingly, this paper is centered on a change of actuator material class which allows the benefits of PBP actuation without the hazard of self-destruction. By using Shape Memory Alloys (SMA) in a PBP configuration, some profound benefits are realized. The first is that even at extremely high deflection levels, self-destruction simply does not occur. The second aids with a fundamental problem possessed by PBP actuators: They are fundamentally inefficient electrical-to-mechanical transducer mechanisms. With a PBP actuator configuration, much of this issue is overcome as efficiency levels are boosted often by an order of magnitude. Finally, the power consumption to hold deflection is reduced by one if not two orders of magnitude. Because aircraft often require flight control surfaces to be held in a given position for extremely long times to trim the vehicle, conventional SMAs are essentially non-starters for many classes of aircraft. This is mainly due

to their speed and dominant irreversible energy loss. Because PBP actuators balance out air and structural loads, the steady-state load on the SMAs is essentially negligible, when properly designed. These advantages of SMAPBP actuators will be explored along with basic structural mechanics, proof-of-concept experiments and correlation.

2. SMAPBP Actuator

The principal design of the actuator was a plate with constant thickness but tapered from root to tip to account for air loads. The actuator plate itself was a composite plate with spring-steel fiberglass epoxy layers. A prove of concept study for this kind of SMA actuated PBP actuator was undertaken in reference [43]. The actuators were designed to function with an applied axial buckling load close to the perfect column buckling load of the actuator itself. The test specimen consisted of a tapered composite plate with a spring steel substrate and two 45 ° glass fiber epoxy composite layers on both sides. The actuator had an overall length of 135 mm with 90 mm of active structure that could be actuated by the SMA wire. Due to the fact that air loads result in high root stresses, the plate itself was tapered from 30 mm at the root to 10 mm at the tip. Preliminary investigations showed that the spring steel substrate available in the lab with a stiffness of 207 GPa and a thickness of 0.127 mm was appropriate to use in the selected design. To actuate the steel composite plate, SMA filaments were attached to the top and bottom of the composite plate. An SMA wire with a 0.254-millimeter diameter, with a stiffness of 75 GPa in the austenitic and 28 GPa in the martensitic state, was selected. An SMA actuation wire of 0.254 millimeter diameter Dynalloy Flexinol [60] was used in these experiments. Prior to the assembly of the actuator, the shape memory alloy wire was prestrained to 2500 μs train plastic strain. The glass fiber layers had the only purpose to create a nonconductive layer between the spring steel substrate and the conductive SMA wire. The 45 °orientation was chosen to minimize the impact of the glass fiber layer on the overall stiffness of the plate. The glass fiber cloth layers had a stiffness of 4.519 GPa and a thickness of 0.222 mm for each of the four glass fiber layers.
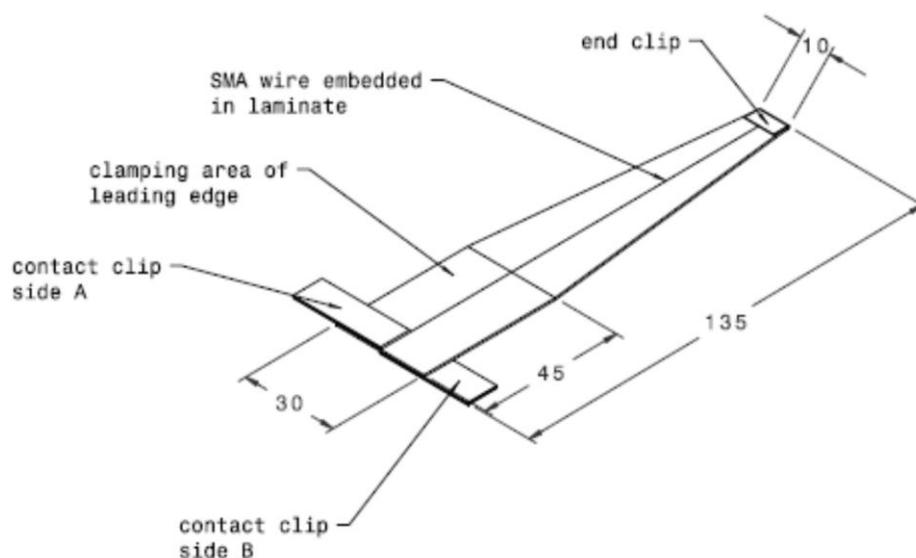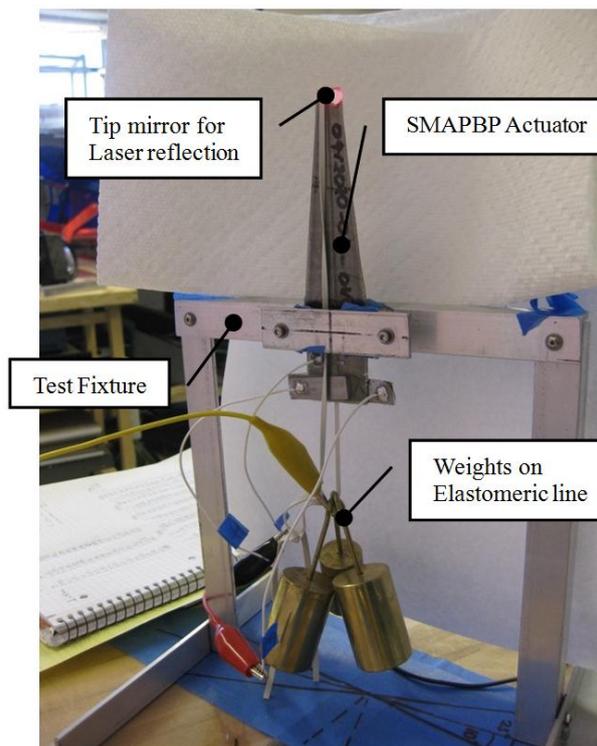

Figure 1. SMAPBP actuator.

The atomic structure changes from Martensite to Austenite by applying heat to the SMA wire. This atomic structure change results in a contraction of the SMA wire and the plate starts to bend. Movement of the SMA wire was suppressed by a clamped steel plate (tip clip) at the tip and a welded steel clip (contact clip) at the root of the test specimen. One single SMA wire was used for actuation of both sides; it was threaded through a transfixion at the tip of the SMAPBP specimen and fixed by a clamped steel plate close to the root of the specimen, the contact clips. The steel substrate served as an electrical conductor in order to produce a closed electrical circle. This arrangement made it possible to actuate both sides separately. For actuation of one side electric power was applied between one of the contact clips and the steel substrate. The steel substrate and the SMA wire were conductively connected by the tip clip (Figure 1).

Due to the observations made in former actuator design steps, it was a natural progression to place the SMA on top of the composite substrate. To prevent the SMA wire from interfering with the bond line between actuator and leading edge, the SMA wire was integrated into the composite at the leading edge. The SMA wire was embedded between two layers of glass fiber epoxy cloth at the clamping area. The 90 mm active length gave the airfoil with integrated actuator an overall length of 150 mm with a 60 mm long leading edge.

2.1. Experimental Set-Up

The test specimen was clamped into the test apparatus in a vertical position. To simulate the axial buckling force F_a, an elastic band with weights was attached to the tip of the test specimen. The band ran along the whole length of the specimen, weights could easily be added under the test specimen (see Figure 2).


Figure 2. SMAPBP actuator clamped in test fixture to measure tip rotation.

The specimen was loaded in 100 g steps which led to axial force steps of approximately 1 N. A mirror at the tip of the actuator was used to measure the tip rotation of the specimen. A laser beam from a light source leveled to the height of the tip was reflected to a displacement measuring device in the distance (Figure 2). This test setup made it possible to measure the tip rotation angle accurately. By applying an electric current on either the top or the bottom SMA wire, the SMA wire started to heat up and therefore contract, the SMAPBP actuator started to bend.

2.2. Results

Figure 3 clearly shows a trend to higher tip rotation angles by increasing the applied axial load. The figure also shows that the displacement with no applied current increases with increasing axial force, this may be caused by bending and buckling phenomena from the applied axial load. The slope of the curves for the different load cases followed also the same pattern. The actuator had nearly no response in the first part of the slope (0 A < I < 0.4 A), followed by a steep rise (0.4 A < I < 0.75 A) and a plateau phase where the tip rotation angle seems to reach a maximum in the order of 55 ° to 70 ° dependent on the applied buckling load.
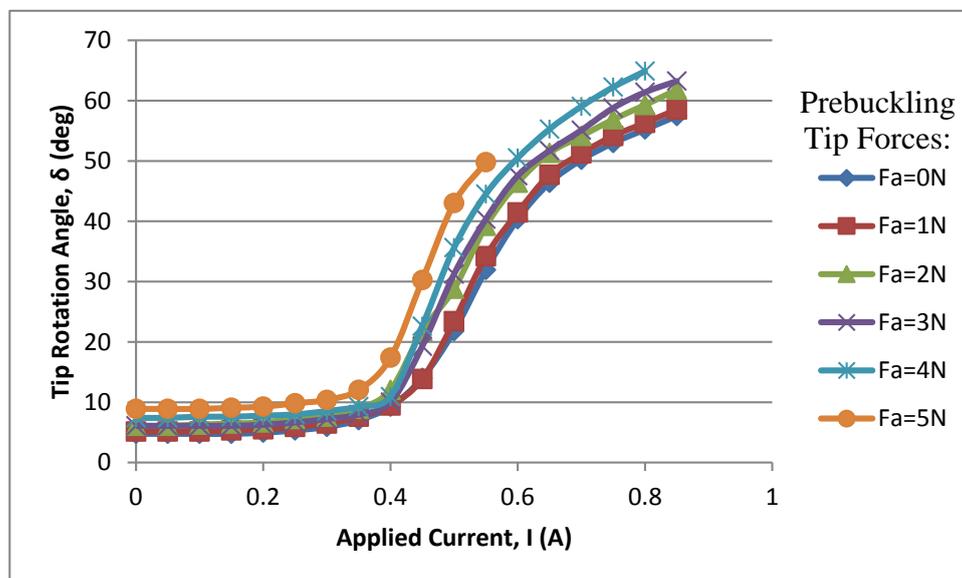
Figure 3. Experimental data: tip rotation angle over applied current.

Figure 3 shows the experimental data for the tip rotation over the applied buckling force F_a for the non-actuated case and the actuated case. The figure shows that the test specimen already had a tip rotation of 4.76 ° at the start of the experiment without any axial load; this displacement may be caused by the hysteresis of the SMA wire after test actuation prior to the experiment. By subtracting the displacement caused by the external axial force with the displacement due to actuation of the wire, an improvement of 33.5% of tip rotation angle could be obtained by using the Post-Buckled Precompressed (PBP) mechanism in comparison of using the specimen without any externally applied load. An improvement of up to 50.5% of tip rotation angle could be achieved with higher current levels, but due to the fact that the control system described later could only provide a maximum actuation current of I = 0.6 A, the 0.55 A case seemed to be the right fit for the proposed application in the airfoil. Experiments also showed

that the SMAPBP actuator can achieve blocked force values of up to 0.45 N. Axial buckling force measurement as a function of finite rotation angles. Measuring the initiating buckling force at finite rotation angles presented nontrivial challenges as the ensuing events were dynamic in nature (as opposed to static). Still, once the initiation force levels were applied and the structure settled in a quiescent shape, the axial buckling force could be compared to finite tip rotation levels as shown in Figure 3.

3. Airfoil

The airfoil intended to prove the concept of a SMAPBP actuator actuated airfoil was proposed to have a chord length of 150 mm and a width of 100 mm. As a basis for the modeling of the airfoil, the NACA profile series was considered. The decision was made to use the NACA 0012 profile because of the large amount of available research data for this airfoil. The symmetric airfoil was used because this paper focuses more on the capabilities of the actuator integrated in the airfoil then maximizing the aerodynamic performance (airfoil profile design). The first 60 mm of the profile were used as a D-spar composite leading edge with the last 90 mm being the actuated length. This decision led to a 40% leading edge and 60% actuator distribution in respect to the overall length of the airfoil.

Figure 4 shows the assembly of the airfoil without the skin. The airfoil structure basically consisted of four main components; the carbon fiber composite leading edge, the actuators, the trailing edge and the elastic latex skin. The leading edge was based on the shape of a NACA0012 [61] airfoil with a chord length of 150 mm. In order to obtain a smooth crossover between the leading edge contour and the straight skin to the trailing edge, a rounded edge was designed at the end of the leading edge. At a distance of 48 mm from the leading edge, a rounded chamfer was used to smoothen the crossover.
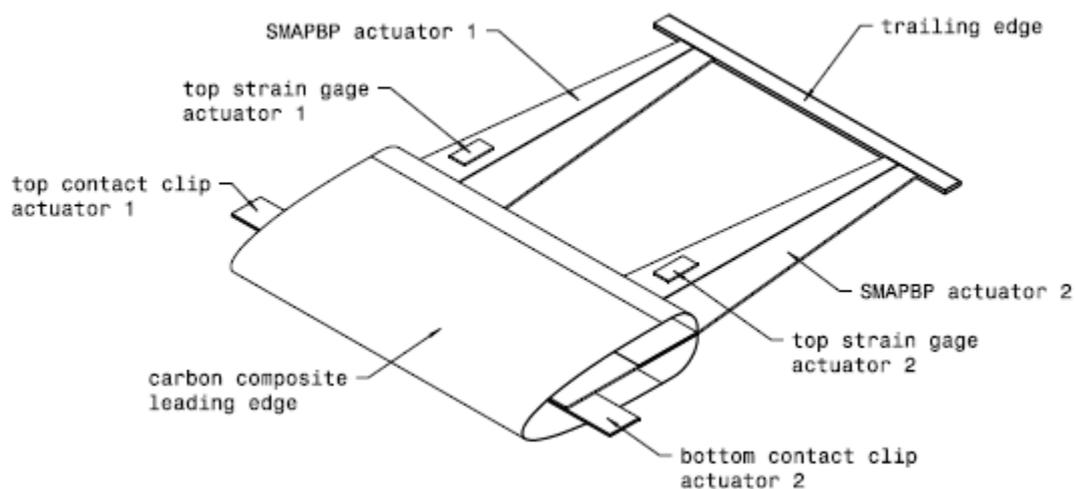
Figure 4. Drawing of assembled airfoil without applied skin.

The SMAPBP actuator was clamped and bonded to the inside of the leading edge at the ends of the carbon composite layer. This design approach made it possible to use the entire chord length of the airfoil more effectively because the clamping area of the actuator was integrated into the substructure of the leading edge and not behind the leading edge. This approach led to a higher actuated length and therefore larger trailing edge displacements.

The trailing edge consisted of a simple bended steel sheet. The trailing edge had the only purpose to connect the two actuators and to obtain a fixture for the applied skin. The trailing edge had an overall length of 100 mm (similar to the width of the leading edge), a thickness of 0.127 mm and a width of 5 mm. Figure 5 shows the manufactured airfoil with attached elastic skin.
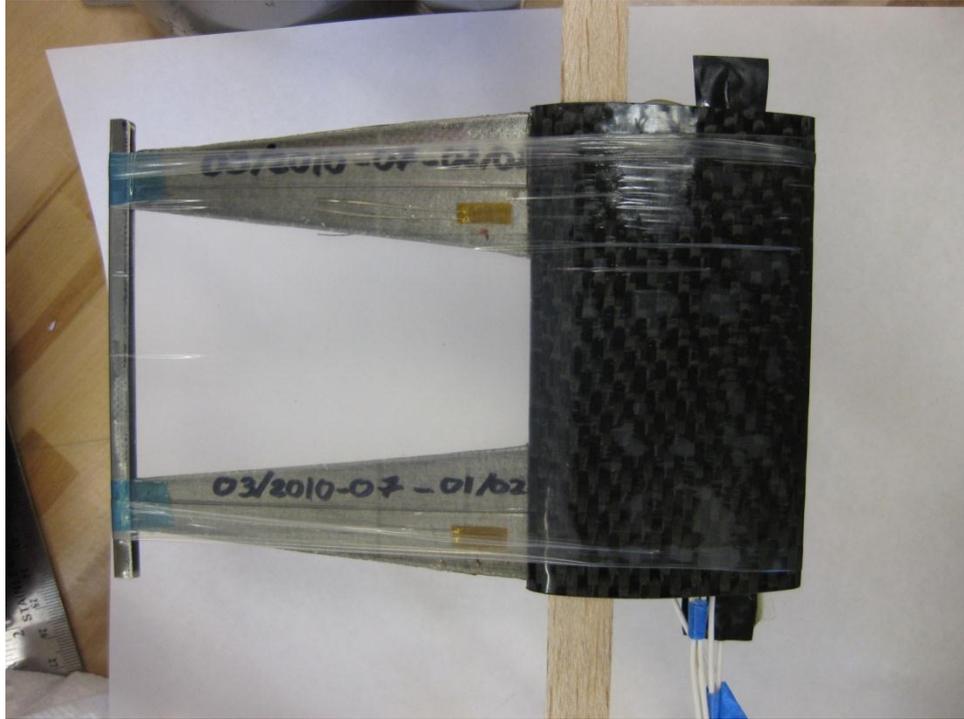

Figure 5. Manufactured airfoil with elastic skin.

The skin had the purpose to give the airfoil a smooth surface and to apply the necessary buckling load to the SMAPBP actuator. The skin consisted of a 100 mm long and 40 mm wide latex tube. Based on tensile tests, an applied axial load of F_{askin} of the skin between 6 N and 8 N was measured, which was just below the Euler buckling loads both computed and experimentally observed.

3.1. Adaptive Shape Change of Airfoil

With simple trigonometric relationships the form change of the airfoil can be modeled mathematically. Figures 6 and 7 show the entire airfoil with leading edge, actuator and skin for variable actuator tip rotation angles. The skin covers the whole outline of the airfoil. The following figures show the shape of the airfoil for actuator tip rotation angles of $\delta = 0°$ and $\delta = 30°$.
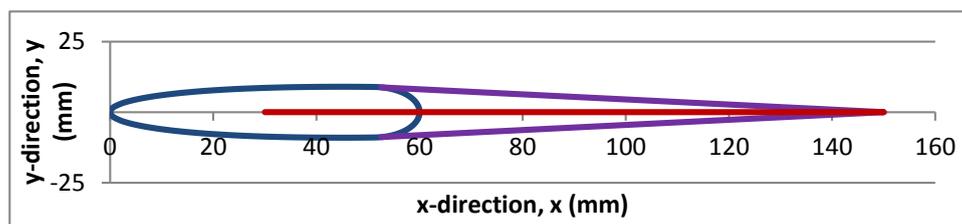

Figure 6. Airfoil cross section at $\delta = 0°$.
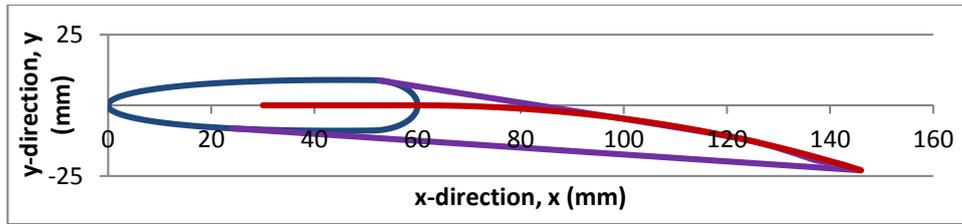
Figure 7. Airfoil cross section at δ = 30 °.

3.2. Active Position Feedback System

Due to the highly hysteretic and nonlinear behavior of the shape memory alloy actuator, it was necessary to introduce an active position feedback system to the airfoil. The control system had the function to control the tip displacement over the applied actuator current. Different concepts for the feedback system were considered and the decision was made to use strain gages to measure the variation of strain on the surface of the actuator.

The strain on the surface correlates directly to the curvature of the actuator and therefore to the tip rotation angle. Figure 8 shows the principle architecture of the active position feedback system proposed for the airfoil. For the proposed airfoil the strain gage in a Wheatstone bridge is used as sensor while the actuator is the actual SMAPBP actuator with current amplifier and the controller which is the control routine is developed in Labview®.
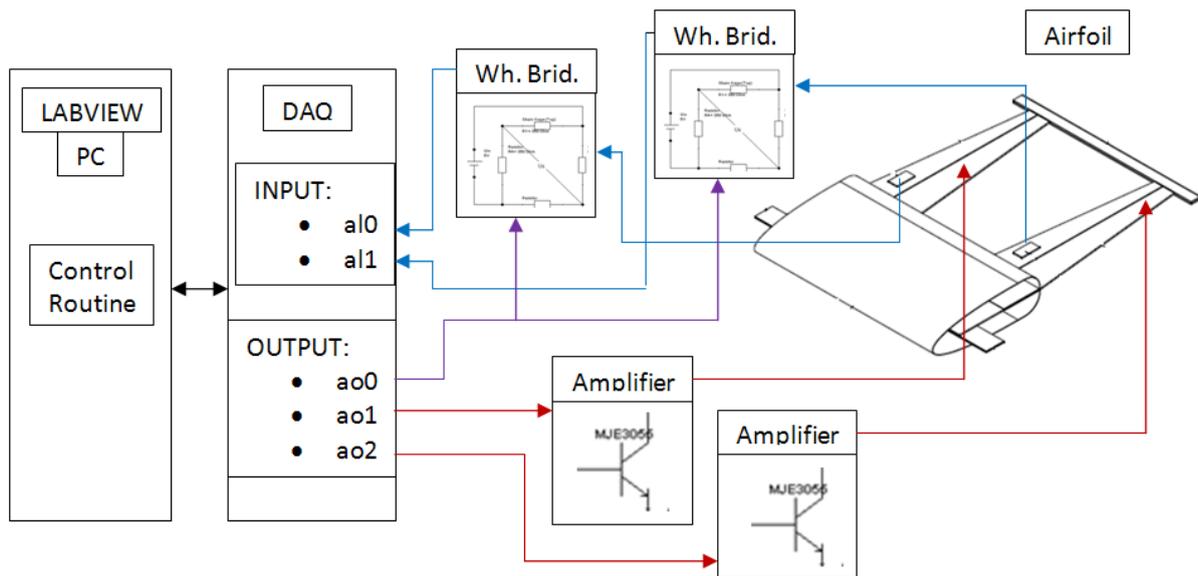
Figure 8. Position feedback system architecture.

By displacing the trailing edge, the resistance of the strain gages applied on the actuators changed. The sensor (strain gage and Wheatstone bridge) senses a change in voltage that was then read into the analog input channels of the data acquisition system (DAQ). The DAQ system was connected over a USB port to a personal computer with Labview® application. The control routine simply minimizes the difference between current and desired position.

Due to the fact that Labview® only provides a variable voltage output and that a variable current level was needed to actuate the actuator's SMA wires, a current amplifier needed to be interposed. With this simple position feedback loop it was possible to overcome the nonlinear hysteretic behavior of the SMA wire and made it possible to command the trailing edge of the airfoil to a specific predetermined displacement.

3.3. Wind Tunnel Tests

Wind tunnel tests were undertaken in the open circuit 31×46 cm wind tunnel at The University of Kansas, which possesses a turbulence factor of 1.1. The purpose of the wind tunnel tests was to prove the performance of the airfoil in a real life application. The wind tunnel tests should prove if the SMAPBP actuator could be able to displace the trailing edge and increase the lift due to actuation. The performance of the airfoil was evaluated for different angles of attack and different actuator tip angle rotations. Figure 9 shows the airfoil in the wind tunnel in an unactuated state before the commencement of the tests.

Figure 9. Side view of airfoil in wind tunnel.

Measurements were taken for actuator tip rotation angles of $\delta = 0°$, $\delta = 10°$, $\delta = 20°$ and $\delta = 30°$ with angles of attack of $\alpha = 0°$, $\alpha = 2°$, $\alpha = 6°$ and $\alpha = 10°$. For each angle of attack the measurements of the four tip rotation were undertaken. After each angle-of-attack measurement, the wind tunnel was turned off and a new angle of attack was adjusted.

Figure 10 shows the actuated airfoil; the white wires are for the actuation of the SMAPBP actuator and the brown wires are from the strain gages applied to the actuators. The SMAPBP actuator performed well during the wind tunnel tests, the trailing edge was displaced up to $\delta = 30°$. The behavior of the airfoil in the wind tunnel seemed different than without any applied air flow. A noticeable difference

was seen in the power consumption of the actuators. The consumption with airflow was significantly higher than without any airflow. Without any airflow an actuator tip rotation angle of $\delta = 30\,°$ could be achieved with 0.6 A actuation current, during the wind tunnel tests a actuation current of up to 1.0 A needed to be applied to achieve similar displacements. This effect might be caused by convectional cooling of the SMA actuator wires by the surrounding airflow. Due to the fact that the airfoil did not have side panels, air flow could enter into the airfoil and cool down the SMA wires.

Figure 10. Side view of Airfoil in Wind Tunnel with a Tip Rotation of $\delta = 30\,°$.

The wind tunnel experiments obtained also lift and drag coefficients for the different actuator tip angle rotations and angles of attack.
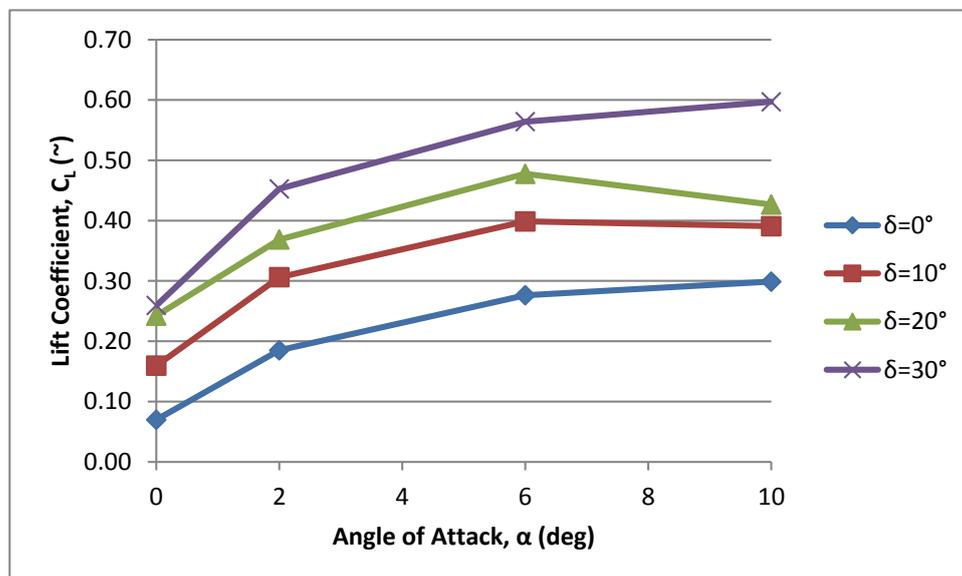
Figure 11. Lift coefficient over angle of attack from wind tunnel experiments.

Figure 11 shows the lift coefficient over various angles of attack and actuator tip displacement angles. The figure shows that the lift increased with an increasing angle of attack α and increasing actuator tip rotation angle δ. The values for the lift coefficient for an angle of attack of $\alpha = 6°$ and $\alpha = 10°$ had similar values. For an actuator tip rotation angle of $\delta = 20°$, the lift coefficient of the $\alpha = 10°$ case was even smaller than the $\alpha = 6°$.

Nevertheless, the wind tunnel tests proved that the airfoil was working under operating conditions. The experiments showed that the lift can be increased substantially by actuating the SMAPBP actuator. The wind tunnel experiments also showed that the SMAPBP actuator can overcome the aerodynamic loads and displace the trailing edge.

4. Conclusions

The Post-Buckled Precompressed (PBP) amplification techniques works well with antagonistically arranged SMA bender beams of the SMAPBP actuator. A 135 mm long steel-fiberglass-epoxy composite actuator was actuated by a pair of 0.254 mm diameter Dynalloy Flexinol wires. The SMAPBP actuator design presented in this paper is capable of achieving high tip displacements and rotations. The specimen demonstrated deflection levels in excess of $120°$ peak-to-peak, representing a deflection growth of 50.5% at axial loads of 5 N. Currently, the actuator is optimized for a buckling force of around 3.5 N–4.5 N and an actuated/buckling length of 90 mm. Therefore, the work presented in this paper can serve as a basic design study for future SMAPBP actuators for other load cases and applications. With the employment of the SMAPBP actuator in an airfoil, the concept of an adaptive flap system with SMA actuation and applied PBP mechanism was presented. Experiments showed that the SMAPBP actuator can achieve high trailing edge displacements and overcome blocked forces originating from airloads. Wind tunnel experiments showed that the airfoil was working well in flight conditions and that the SMAPBP actuator was able to overcome the aerodynamic loads introduced by the air flow.

Author Contributions

The authors contributed equally to this paper.

Conflicts of Interest

The authors declare no conflict of interest.

References

1. Crawley, E.; Lazarus, K.; Warkentin, D. Embedded actuation and processing in intelligent materials. In Proceedings of the 2nd International Workshop on Composite Materials and Structures for Rotorcraft, Troy, NY, USA, 14–15 September 1989.

2.   Lazarus, K.; Crawley, E. Multivariable active lifting surface using strain actuation: analytical and experimental results. In Proceedings of the Third International Conference on Adaptive Structures, San Diego, CA, USA, 9–11 November 1992.

3.   Lazarus, K.; Crawley, E.; Bohlmann, J.D. Static aerolastic control using strain actuated adaptive structures. *J. Intell. Mater. Syst. Struct.* **1991**, *2*, 386–410.

4.   Spangler, R.L.; Hall, S.R. Piezoelectric actuators for helicopter rotor control. In Proceedings of the 31st Structures, Structural Dynamics and Materials Conference, Long Beach, CA, USA, 2–4 April 1990.

5.   Barrett, R. Intelligent rotor blade actuation through directionally attached piezoelectric crystals. In Proceedings of the 46th AHS National Conference and Forum, Washington, DC, USA, 21–23 May 1990.

6.   Barrett, R. Intelligent Rotor Blade and Structures Development using Piezoelectric Crystals. Master's Thesis, the UM, College Park, MD, USA, 1990.

7.   Barrett, R. Method and Apparatus for Sensing and Actuating in a Desired Direction. U.S. Patent 5,440,193, August 1995.

8.   Barrett, R. Actuation strain decoupling through enhanced directional attachment in plates and aerodynamic surfaces. In Proceedings of the First European Conference on Smart Structures and Materials, Glasgow, UK, 12–14 May 1992; pp. 383–386.

9.   Ehlers, S.M.; Weisshaar, T.A. Static Aeroelastic Behavior of an Adaptive Laminated Piezoelectric Composite Wing. In Proceedings of the 31st Structures, Structural Dynamics, and Materials Conference, Long Beach, CA, USA, 2–4 April 1990; pp. 1611–1623.

10. Ehlers, S.M.; Weisshaar, T.A. Adaptive wing flexural axis control. In Proceedings of the Third International Conference on Adaptive Structures, San Diego, CA, USA, 9–11 November 1992.

11. Ehlers, S.M.; Weisshaar, T.A. Effects of material properties on static aerolastic control. In Proceedings of the 33rd Structures, Structural Dynamics and Materials, Dallas, TX, USA, 13–15 April 1992.

12. Barrett, R. Active plate and missile wing development using dap elements. *AIAA J.* **1994**, *32*, 601–609.

13. Barrett, R. Active plate missile development using EDAP elements. *J. Smart Mater. Struct.* **1992**, *1*, 214226.

14. Barrett, R. Active composite torque-plate fins for subsonic missiles. In Proceedings of the Dynamic Response of Composite Structures Conference, New Orleans, LA, USA, 20 August–1 September 1993.

15. Barrett, R. *Advanced low-Cost Smart Missile Fin Technology Evaluation*; Report to the USAF Armament Directorate, Eglin Air Force Base: Eglin, FL, USA, 1993.

16. Barrett, R.; Brozoski, F.; Gross, R.S. Design and testing of a subsonic all-moving adaptive flight control surface. *AIAA J.* **1997**, *35*, 1217–1219.

17. Barrett, R.; Brozoski, F. Missile flight control using active flexspar actuators. *J. Smart Mater. Struct.* **1996**, *5*, 121–128.

18. Barrett, R. Active aeroelastic tailoring of an adaptive flexspar stabilator. *J. Smart Mater. Struct.* **1996**, *5*, 723–730.

19. Barrett, R. *Invention and Evaluation of the Barrel Launched Adaptive Munition (BLAM)*; Final report for USAF contract no. F-49620-93-C-0063, USAF Wright Laboratory Flight Vehicles Branch: Wright-Patterson AFB, OH, USA, 1995.

20. Barrett, R.; Stutts, J. *Barrel-Launched Adaptive Munition BLAM Experimental Round Research*; Final report for USAF contract no. F-49620-93-C-0063, USAF Wright Laboratory Flight Vehicles Branch: Wright-Patterson AFB, OH, USA, 1997.

21. Winchenbach, G. *Cone Aerodynamic Test*; Aeroballistic Research Facility Ballistic Spark Range Technical Report; USAF Wright Laboratory Flight Vehicles Branch: Wright-Patterson AFB, OH, USA, 1996.

22. Barrett, R.; Stutts, J. Modelling, Design and testing of a barrell-launched adaptive munition. In Proceedings of the 4th Annual SPIE Symposium on Smart Structures and Materials, San Diego, CA, USA, 3–6 March 1997.

23. Barrett, R. *Design, Construction and Testing of a Prrof-of-Cncept Smart Compressed Reversed Adaptive Munition*; SCRAM Report, Final Report to the USAF Armament Directorate, Wright Laboratory: Eglin AFB, FL, USA, 1996.

24. Barrett, R.; Stutts, J. Development of a piezoceramic flight control surface actuator for highly compressed munitions. In Proceedings of the 39th Structures, Structural Dynamics and Materials Conference, Long Beach, CA, USA, 20–23 April 1998.

25. Barrett, R. *Construction and Test Report for a Rotationally Active Linear Actuator (RALA) Adaptive Canard*; Final Report for McDonnell Douglas: St. Louis, MO, USA, 1997.

26. Knowles, G.; Barrett, R.; Valentino, M. Self-contained high authority control of miniature flight control systems for aera dominace. In Proceedings of the SPIE 11th International Symposium on Smart Structures and Materials, San Diego, CA, USA, 14–18 March 2004.

27. Lee, G. *Range-Extended Adaptive Munition (REAM)*; Final Report from Lutronix Corporation to the DARPA: Del Mar, CA, USA, 1999.

28. Lee, G. *40/50 Caliber Range-Extended Adaptive Munition (REAM)*; Final Report from Lutronix Corporation to the US Army TACOM-ARDEC: Del Mar, CA, USA, 2000.

29. Rabinovitch, O.; Vinson, J.R. On the design of piezoelectric smart fins for flight vehicles. *J. Smart Mater. Struct.* **1993**, *12*, 686–695.

30. Barrett, R. *High Bandwith Electric Rotor Blade Actuator Study*; Phase I SBIR proposal submitted to the U.S. Army Aviation System Command: St. Louis, MO, USA, 27 June 1992.

31. Barrett, R.; Stutts, J. Design and testing of a 1/12th scale solid state adaptive rotor. *J. Smart Mater. Struct.* **1997**, *6*, 686–695.

32. Barrett, R.; Frye, P.; Schliesman, M. Design, constructionand characterization of a flightworty piezoelectric solid state adaptive rotor. *J. Smart Mater. Struct.* **1998**, *7*, 422–431.

33. Lee, G. *Design and Testing of the Kolibri Vertical Take-Off and Landing Micro Aerial Vehicle*; Final report to the Department of Defense CounterDrug Technology Office: Washington, DC, USA, 1997.

34. Barrett, R.; Howard, N. Adaptive aerostructures for subscale aircraft. In Proceedings of the 20th Southeastern Conference on Theoretical and Applied Mechanics, Pine Mountains, GA, USA, 17 April 2000.

35. Lesieutre, G.A.; Davis, C.L. Can a Coupling Coefficient of a Piezoelectric Actuator be Higher than its Active Material? *J. Intell. Mater. Syst. Struct.* **1997**, *8*, 859–867.

36. Lesieutre, G.A.; Davis, C.L. Transfer Having a Coupling Coefficient Higher than its Active Material. U.S. Patent 6,236,143, 22 May 2001.

37. Barrett, R.; Tisco, P. PBP Adaptive Actuator Device and Embodiments. International Patent Application Number PCT/NL2005/000054, via TU Delft, 18 February 2005.

38. Barrett, R.; Vos, R.; Tisco, P.; De Breuker, R. Post-Buckled Precompressed (PBP) Actuators: Enhancing VTOL Autonomous High Speed MAVs. In Proceedings of the 13th AIAA/ASME/AHS Adaptive Structures Conference, Austin, TX, USA, 18–21 April 2005.

39. Vos, R.; De Breuker, R.; Barrett, R.; Tisco, P. Morphing Wing Flight Control via Post-Buckled Precompressed Piezoelectric Actuators. *AIAA J. Aircr.* **2007**, *44*, 1060–1068.

40. Barrett, R.; McMurtry, R.; Vos, R.; Tisco, P.; De Breuker, R. Post-Buckled Precompressed Pieyoelectric Flight Control Actuator Design, Development and Demonstration. *J. Smart Mater. Struct.* **2006**, *15*, 1323–1331.

41. De Breuker, R.; Vos, R.; Barrett, R.; Tisco, P. Nonlinear Semi-Analytical Modeling of Post-Buckled Precompressed (PBP) Piezoelectric Actuators for UAV Flight Control. In Proceedings of the 47th AIAA/ASME/ASCE/AHS/ASC Structures, Structural Dynamics and Materials Conference 14th AIAA/ASME/AHS Adaptive Structures Conference, Newport, RI, USA, 1–4 May 2006.

42. Van Schravendijk, M.; Groen, M.; Vos, R.; Barrett, R. Closed Loop Control for High Bandwidth, High Curcature Post-Buckled Precompressed Actuators. In Proceedings of the 50th AIAA/ASME/ASCE/AHS/ASC Structures, Structural Dynamics, and Materials Conference 17th AIAA/ASME/AHS Adaptive Structures Conference 11th AIAA No, Palm Springs, CA, USA, 4–7 May 2009.

43. Arrieta, A.F.; Bilgen, O.; Friswell, M.I.; Hagedorn, P. Passive load alleviation bi-stable morphing concept. *AIP Adv.* **2012**, *2*, doi:10.1063/1.4739412.

44. Bilgen, O.; Friswell, M.I. Implementation of a Continuous-Inextensible-Surface Piezocomposite Airfoil. *J. Aircr.* **2013**, *50*, 508–518.

45. Friswell, M.I.; Ali, S.F.; Bilgen, O.; Adhikari, S.; Lees, A.W.; Litak, G. Nonlinear Piezoelectric Vibration Energy Harvesting from an Inverted Cantilever Beam with Tip Mass. *J. Intell. Mater. Syst. Struct.* **2012**, *23*, 1505–1521.

46. Arrieta, A.F.; Bilgen, O.; Friswell, M.I.; Hagedorn, P. Morphing dynamic control for bi-stable composites. *J. Intell. Mater. Syst. Struct.* **2012**, doi:10.1177/1045389X12449918.

47. Bilgen, O.; Butt, L.M.; Day, S.R.; Sossi, C.A.; Weaver, J.P.; Wolek, A.; Mason, W.H.; Inman, D.J. A Novel Unmanned Aircraft with Solid-State Control Surfaces: Analysis and Flight Demonstration. *J. Intell. Mater. Syst. Struct.* **2012**, doi:10.1177/1045389X12459592.

48. Borowiec, M.; Litak, G.; Friswell, M.I.; Ali, S.F.; Adhikari, S.; Lees, A.W.; Bilgen, O. Energy Harvesting in Piezoelastic Systems Driven by Random Excitations. *Int. J. Struct. Stab. Dyn.* **2012**, doi:10.1142/S0219455413400063.

49. Arrieta, A.F.; Bilgen, O.; Friswell, M.I.; Hagedorn, P. Modeling and configuration control of multi-stable piezoelectric composites. *Smart Mater. Struct.* **2013**, submitted for publication.

50. Bilgen, O.; Wang, Y.; Inman, D.J. Electromechanical Comparison of Cantilevered Beams with Multifunctional Piezoceramic Devices. *Mechan. Syst. Signal Process.* **2012**, *27*, 763–777.

51. Karami, M.A.; Bilgen. O.; Inman, D.J.; Friswell, M.I. Experimental and Analytical Parametric Study of Single Crystal Unimorph Beams for Vibration Energy Harvesting. *Trans. Ultrason. Ferroelectr. Freq. Control* **2011**, *58*, 1508–1520.

52. Bilgen, O.; Inman, D.J.; Friswell, M.I. Theoretical and Experimental Analysis of Hysteresis in Piezocomposite Airfoils Using the Classical Preisach Model. *J. Aircr.* **2011**, *48*, 1935–1947.

53. Barbarino, S.; Bilgen, O.; Ajaj, R.M.; Friswell, M.I.; Inman, D.J. A Review of Morphing Aircraft. *J. Intell. Mater. Syst. Struct.* **2011**, *22*, 823–877.

54. Bilgen, O.; Karami, M.A.; Inman, D.J.; Friswell, M.I. The Actuation Characterization of Cantilevered Unimorph Beams with Single Crystal Piezoelectric Materials. *Smart Mater. Struct.* **2011**, *20*, doi:10.1088/0964-1726/20/5/055024.

55. Bilgen, O.; De Marqui Junior, C.; Kochersberger, K.B.; Inman, D.J. Macro-Fiber Composite Actuators for Flow Control of a Variable Camber Airfoil. *J. Intell. Mater. Syst. Struct.* **2011**, *22*, 81–91.

56. Bilgen, O.; Kochersberger, K.B.; Inman, D.J.; Ohanian, O.J. Macro-Fiber Composite Actuated Simply-Supported Thin Morphing Airfoils. *Smart Mater. Struct.* **2010**, *19*, doi:10.1088/0964-1726/19/5/055010.

57. Bilgen, O.; Erturk, A.; Inman, D.J. Analytical and Experimental Characterization of Macro-Fiber Composite Actuated Thin Clamped-Free Unimorph Benders. *J. Vib. Acoust.* **2010**, *132*, doi:10.1115/1.4001504.

58. Bilgen, O.; Kochersberger, K.B.; Inman, D.J.; Ohanian, O.J. Novel, Bi-Directional, Variable Camber Airfoil via Macro-Fiber Composite Actuators. *J. Aircr.* **2010**, *47*, 303–314.

59. Bilgen, O.; De Marqui Junior, C.; Kochersberger, K.B.; Inman, D.J. Piezoceramic Composite Actuators for Flow Control in Low Reynolds Number Airflow. *J. Intell. Mater. Syst. Struct.* **2010**, *21*, 1201–1212.

60. Dynalloy, I. Flexinol™ Technical Data. Available online: http://www.robotshop.com/media/files/pdf/flexinol-technical-data.pdf (accessed on 27 July 2015).

61. Ladson, C.L.; Brooks, C.W., Jr.; Hill, A.S.; Sproles, D.W. Computer program to obtain ordinates for NACA airfoils. *NASA Technical Memorandum*; Available online: http://ntrs.nasa.gov/archive/nasa/casi.ntrs.nasa.gov/19970008124.pdf (accessed on 27 July 2015).